

Infrared emissivity of copper-alloyed spinel black coatings for concentrated solar power systems

I. González de Arrieta^a, T. Echániz^{b,*}, R. Fuente^b, E. Rubin^{c,d}, R. Chen^{c,d}, J.M. Igartua^a, M.J. Tello^a, G.A. López^a

^a Applied Physics II, University of the Basque Country (UPV/EHU), Leioa 48940, Spain

^b Applied Mathematics, University of the Basque Country (UPV/EHU), Bilbao 48013, Spain

^c Materials Science & Engineering, University of California, San Diego, California 92093, USA

^d Mechanical and Aerospace Engineering, University of California, San Diego, California 92093, USA

*Corresponding author.

Email address: telmo.echaniz@ehu.eus (T. Echániz)

Abstract

The directional spectral emissivities of four new copper-alloyed spinel black coatings for concentrated solar power (CSP) applications have been measured in the mid-infrared up to 800 °C and compared to that of the commercial Pyromark 2500® black paint, deposited in the same conditions on Inconel 625 substrates. Stable results were found for all coatings at all temperatures, with similar spectral features at the desired working temperatures. The temperature and angular dependences have been discussed and related to the morphology of the samples. The integrated total hemispherical emissivity increases up to 400 °C for all coatings and then stabilizes, with similar values for most materials, with the exception of the porous $\text{Cu}_{0.5}\text{Cr}_{1.1}\text{Mn}_{1.4}\text{O}_4$ coating. This coating offers a reduced total hemispherical emissivity due to increased semitransparency at high angles arising from its porous structure. This porosity has also been linked to an increase in both the solar absorptance and the emissivity in the normal direction due to enhanced light trapping, which means that this coating shows signs of both spectral and directional selectivity. The results contained in this work, together with the significant dispersion of literature data reported for Pyromark, support the idea that structural properties are key for the high-temperature emissivity of the coatings and highlight the importance of direct experimental characterization of the emissivity of coatings. Combined with solar absorptance measured in the usual manner, these direct angle-resolved emissivity measurements allow for more accurate calculations of the real efficiencies of the coatings at high temperature.

Keywords: infrared emissivity, solar absorbing coating, tandem structure, porous materials, concentrated solar power, conversion efficiency

1. Introduction

Concentrated solar power (CSP) is an alternative energy source with great potential due to easy integration with thermal energy storage systems to avoid intermittence of supply [1]. In order to improve their Carnot efficiency, CSP plants require operation at higher temperatures [2],

where radiative heat transfer becomes increasingly dominant, and knowledge of the thermal radiative properties of solar-absorbing coatings becomes crucial.

A number of strategies for improving the efficiency of solar energy harvesting in solar thermal plants have been devised. This includes approaches such as spectrally selective metal-dielectric multilayers or micro/nanostructured surfaces tailored for efficient light trapping [3]. However, these materials are often expensive to develop and most are not expected to be stable enough for use in the desired operating conditions of future solar power tower plants (~750 °C in air). Therefore, simpler attempts such as the manufacturing of porous structures may become promising alternatives for tuning their optical properties and improving the overall efficiency in a cost-effective manner [4-6].

Currently, the most widely adopted solar absorber coating for central tower plants is a commercial black paint known as Pyromark 2500® (hereafter referred to as Pyromark). This paint is easy to deposit and shows good optical properties, but it is susceptible to aging at high temperatures, which significantly reduces its solar-to-thermal conversion efficiency over time [7]. In order to fulfill the goals set in the SunShot Initiative of increasing the working fluid temperature at 720 °C detailed in the latest Roadmap in 2017 [8], the next-generation solar absorbers must be stable at temperatures around 800 °C, which motivates the development of alternatives to Pyromark based on more stable oxide-based materials, such as spinels [9,10]. These materials have been widely characterized in the literature and offer improved thermal and optical capabilities, together with an easily scalable fabrication process by spray coating.

Good emissivity characterization is one of the key requirements for successful application of the materials described above, as has been exemplified in studies of solar selective coatings designed for parabolic trough CSP systems [11-13]. In this respect, direct emissivity measurements in high-emissivity coatings constitute an important topic in infrared radiometry [14-19]. However, these measurements can become a challenging task due to a combination of factors related to the temperature measurements of the sample surface and the blackbody reference, as well as possible thermal gradients [18,19]. Furthermore, the emissivities of coatings may be affected by extrinsic factors such as non-homogeneous microstructures and surfaces, differences in curing processes or aging effects, which make comparisons between experimental results difficult, even for samples of the same material. These factors help to explain the discrepancies among the reported values of the emissivity of Pyromark in the literature [7,20-24]. Therefore, a systematic review and characterization of the range of variability and the effect of extrinsic parameters of these materials is key for their application. Moreover, directional emissivity data and reliable uncertainties are often lacking in the literature concerning this type of materials [17].

This work presents high-temperature emissivity measurements performed by a direct method on a new set of solar-absorbing layers based on Cu-alloyed spinel nanoparticles ($\text{Cu}_{0.5}\text{Cr}_{1.1}\text{Mn}_{1.4}\text{O}_4$, CuCr_2O_4 and CuFeMnO_4). These new materials feature higher solar absorptance than that of Pyromark while, at the same time, their crystal structure is better suited for an improved high-temperature stability and long-term durability [10]. The emissivity results are compared to data for Pyromark deposited in the same conditions, as well as to the emissivity of the bare substrate (Inconel 625) acting as a control sample due to possible issues of semitransparency. The main objective of this paper is to study whether these new materials also offer advantageous properties in the infrared region concerning a reduction in thermal radiation losses.

2. Experimental details

2.1. Synthesis and processing of the materials

CuCr_2O_4 and CuFeMnO_4 nanoparticles were synthesized through hydrothermal growth. For the synthesis of CuCr_2O_4 , 1 M of $\text{CuCl}_2 \cdot 2\text{H}_2\text{O}$ was mixed with 2M of $\text{CrCl}_3 \cdot 6\text{H}_2\text{O}$ in de-ionized water for 1.5 hours before adding 10M of NaOH for co-precipitation of Cu-Cr hydroxides. After reaching a pH of 11.5, the solution continued mixing for one additional hour before pouring the solution into a 45 mL Teflon-lined autoclave and placing the autoclave in an oven at 200 °C for 20 hours for hydrothermal growth. After hydrothermal growth, the sample was removed from the oven, freeze-dried, and annealed at 550 °C for 5 hours in air in a tube furnace. Procedure for the synthesis of CuFeMnO_4 was identical, apart from using 1 M of $\text{CuCl}_2 \cdot 2\text{H}_2\text{O}$, $\text{FeCl}_3 \cdot 6\text{H}_2\text{O}$, and $\text{MnCl}_2 \cdot 4\text{H}_2\text{O}$ as precursors.

$\text{Cu}_{0.5}\text{Cr}_{1.1}\text{Mn}_{1.4}\text{O}_4$ nanopowders were purchased from Foshan Huayi Ceramic Colours Co., Ltd. in China. The nanopowders were synthesized through mixing starting metal oxides at high temperature with ball milling until a homogeneous composition was formed.

The procedure to make the nanopowder mixtures for spray coating CuCr_2O_4 and $\text{Cu}_{0.5}\text{Cr}_{1.1}\text{Mn}_{1.4}\text{O}_4$ dense layers was identical. The nanoparticles were mixed with a 4:1 weight ratio (particles/resin) with a solution made of methyl phenyl polysiloxane resin binder (SILIKOPHEN P80/X, Evonik), isobutanol, and xylene. The solution was ball-milled for one day before spray-coating it onto Inconel 625 substrates. After allowing the samples to dry overnight, they were cured in air in a step-wise process from room temperature to 100 °C for 10 minutes, 250 °C for 120 minutes, 550 °C for 180 minutes, 750 °C for 120 minutes, and then naturally cooled to room temperature. The resulting coatings consisted of agglomerated nanoparticles in an amorphous silica matrix and had thicknesses of around 25 μm .

To make porous layers for porous CuFeMnO_4 and $\text{Cu}_{0.5}\text{Cr}_{1.1}\text{Mn}_{1.4}\text{O}_4$, we followed our previous recipe that consisted of adding sacrificial polymer beads to the solution [9,25]. Cross-linked polystyrene beads of 1.3 μm (SX-130H) and acrylic beads of 400 nm (MP2701) were purchased from Soken Chemical & Engineering, added to the solution with a weight ratio of 1.0:0.8:1.1 (particles/beads/resin), and probed via sonicator to promote mixing. Afterward, the coating procedure (ball-milling, spray-coating, curing) was identical to the dense layers. The polymer beads decompose during the step-wise curing process, leaving nano- and micro-sized pores to create a porous layer. The porous CuFeMnO_4 coating was obtained on top of a CuCr_2O_4 layer, whereas the porous $\text{Cu}_{0.5}\text{Cr}_{1.1}\text{Mn}_{1.4}\text{O}_4$ one was produced as a standalone sample directly onto the substrate. The thicknesses obtained were around 5 μm for the former and 25 μm for the latter.

Pyromark black paint (LA-CO), the current state-of-the-art material for solar absorber coatings for CSP solar towers, was obtained to compare emissivity measurements. Pyromark was diluted with xylene and toluene 10% (w/w), spray-coated and cured with the same recipes as mentioned above.

The substrates used for all coatings in this study were made of Inconel 625. One uncoated sample was also prepared for the emissivity measurements and its surface state was studied using a mechanical roughness tester (Mitutoyo SJ-201). The roughness parameters were found to be $R_a=0.23 \mu\text{m}$, $R_q=0.30 \mu\text{m}$, $R_z=1.88 \mu\text{m}$, $R_t = 2.39 \mu\text{m}$ and $RSm = 45 \mu\text{m}$.

2.2. Microstructural and optical characterization

The morphology and particle size of as-cured samples were investigated by scanning electron microscopy (SEM) surface images (Zeiss Sigma 500, acceleration voltage 10 kV). Particle sizes of each coating were measured through ImageJ processing software. The UV/Vis reflectance spectra of the coatings has been measured at room temperature with a Jasco V780 spectrophotometer equipped with a 150 mm integrating sphere coated with Spectrafect. The measured spectral range was 0.20-2.5 μm , with a photometric accuracy of 0.3%. The thermal stability and evolution of the microstructure and solar absorptance of the coatings has been extensively characterized in a previous reference [10]. In the case of the $\text{Cu}_{0.5}\text{Cr}_{1.1}\text{Mn}_{1.4}\text{O}_4$ -based ones, they showed improved solar absorption properties with respect to Pyromark, with very little to no degradation after annealing at 800 °C for 2000 hours.

2.3. Emissivity measurements

The instrumental setup used to perform the emissivity measurements is the HAIRL radiometer, which allows high-accuracy directional spectral emissivity measurements in a controlled atmosphere at high temperatures [26]. Samples are heated using resistor elements, and the surface temperature is measured using two symmetrically located type K thermocouples spot-welded onto the metallic substrate, in an area with ensured good thermal homogeneity. The atmosphere inside the chamber can be controlled using a turbomolecular pump. All measurements in this work have been performed in air, except for that of the substrate, which was measured in a 10^{-4} mbar vacuum. Blackbody measurements have been performed in the corresponding atmospheres to ensure the same optical path for all wavelengths.

Measurements are performed with the blacksur method, while the calibration has been carried out by the modified two-temperature method [27,28]. Combined standard uncertainties (with a coverage factor of $k=1$, 68.27%) of the directional spectral measurements have been computed [29]. Inaccuracies around the atmospheric absorption bands of CO_2 and H_2O have been corrected using the transmittance spectra obtained by measurements on blackbodies in air and in N_2 atmosphere. The accuracy of this correction is estimated as 0.5%.

Directional spectral emissivity measurements were made from 200 to 800 °C every 100 °C for all samples. Aging effects at 800 °C were considered to be negligible due to the short measurement and stabilization times (<1 h) [10]. The spectral range was 2-22 μm , and the measured angles were 10-80°, every 10°. Experimental results together with the electromagnetic theory indicate that the emissivity between 0° and 20° shows a flat angular dependence [30-32]. This fact allows measuring the normal emissivity at 10° and thus avoiding systematic errors arising from parasitic radiations in measurements at 0° [30].

Finally, a numerical integration has also been performed in both wavelength and solid angle to calculate the total hemispherical emissivities from directional spectral data [31]:

$$\varepsilon_H = \frac{1}{\pi} \int_0^{2\pi} \int_0^{\pi/2} \frac{\int_0^{\infty} \varepsilon(\lambda, \theta, T) L(\lambda, T) d\lambda}{\int_0^{\infty} L(\lambda, T) d\lambda} \cos \theta \sin \theta d\theta d\varphi \quad (1)$$

The integration in solid angle required emissivity data at 0° and 90°, which was provided by the electromagnetic theory [31]. In the case of wavelength integration, the extrapolation procedure

outside the measured spectral range relies on the assumption of a monotonic wavelength dependence in the vicinity of the measured range, as explained elsewhere [11]. Estimated values of the standard uncertainties of total hemispherical data have been calculated by propagating the spectral uncertainties inside the numerical integral [33].

3. Results and discussion

3.1. Preliminary characterization

The morphologies after deposition and curing are shown in surface SEM images (Fig. 1). This allows characterizing the shape and particle size of dense $\text{Cu}_{0.5}\text{Cr}_{1.1}\text{Mn}_{1.4}\text{O}_4$, porous $\text{Cu}_{0.5}\text{Cr}_{1.1}\text{Mn}_{1.4}\text{O}_4\text{CuFeMnO}_4$ (porous top)/ CuCr_2O_4 (dense bottom), CuCr_2O_4 , and Pyromark, respectively. CuCr_2O_4 nanoparticles were the smallest and the majority are between 50-100 nm, while CuFeMnO_4 , Pyromark, and $\text{Cu}_{0.5}\text{Cr}_{1.1}\text{Mn}_{1.4}\text{O}_4$ nanoparticles were similarly sized between 100-300 nm. Fig. 2 shows SEM images at lower magnification in order to compare the microstructures of both $\text{Cu}_{0.5}\text{Cr}_{1.1}\text{Mn}_{1.4}\text{O}_4$ coatings (dense and porous). The most significant difference between the two samples involves the presence of larger and deeper pores for the porous sample, with mean diameters in the range of 1-5 μm . This feature results from the decomposition of polymer beads, which have size ranging from 400 nm to 1.3 μm , and allows for more efficient trapping of light in the cavities [9].

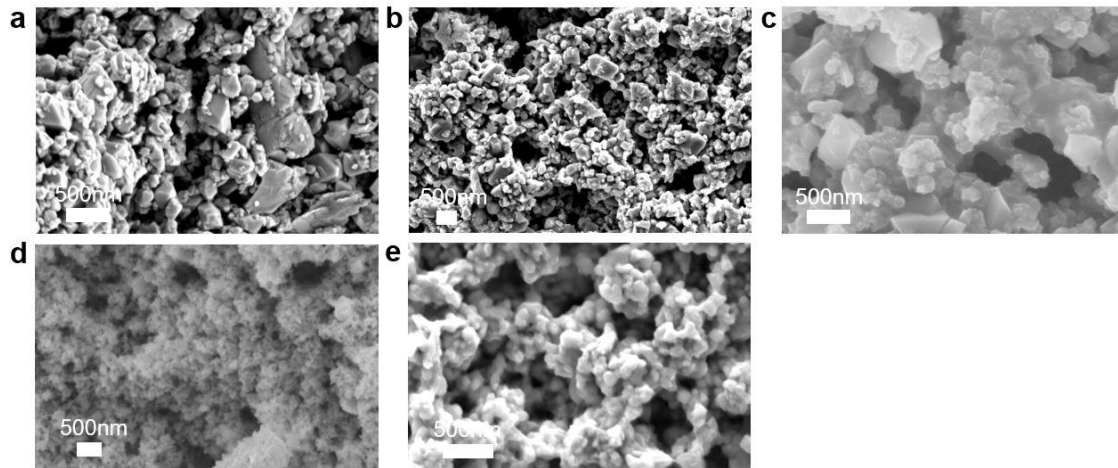


Fig. 1: SEM images of solar absorber coatings (a) dense $\text{Cu}_{0.5}\text{Cr}_{1.1}\text{Mn}_{1.4}\text{O}_4$, (b) dense $\text{Cu}_{0.5}\text{Cr}_{1.1}\text{Mn}_{1.4}\text{O}_4$, (c) CuFeMnO_4 (PT)/ CuCr_2O_4 (DB), (d) CuCr_2O_4 , and (e) Pyromark.

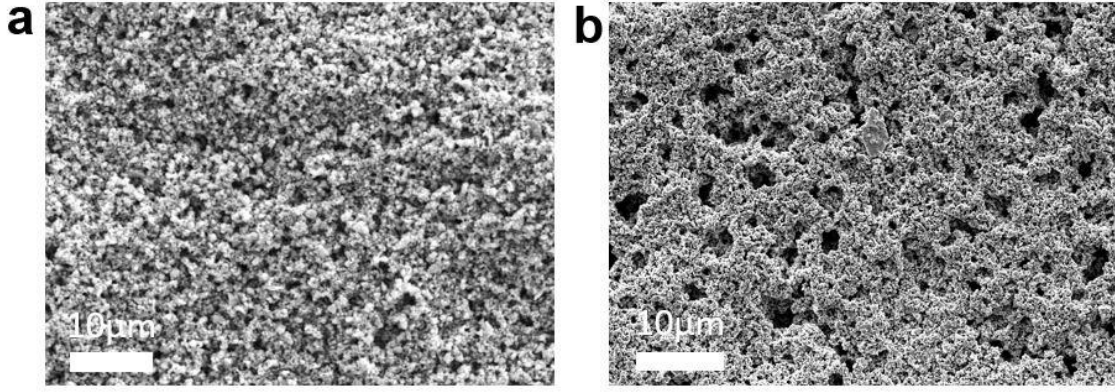


Fig. 2: SEM images of the surface morphologies of both $\text{Cu}_{0.5}\text{Cr}_{1.1}\text{Mn}_{1.4}\text{O}_4$ coatings: (a) dense and (b) porous.

The solar absorptance of the coatings have been calculated by numerical integration of the reflectance data, as seen in Eq. (2). The AM 1.5 Standard Spectrum was used as the source of solar irradiance data. The results are shown in Table 2. They are consistent with results found in [10].

$$\alpha_S = \frac{\int_{0.28}^{4.0} (1-R(\lambda)) I_{AM1.5} d\lambda}{\int_{0.28}^{4.0} I_{AM1.5} d\lambda} \quad (2)$$

Table 2. Solar absorptances of the five solar absorbing coatings.

Pyromark	$\text{Cu}_{0.5}\text{Cr}_{1.1}\text{Mn}_{1.4}\text{O}_4$ (D)	$\text{Cu}_{0.5}\text{Cr}_{1.1}\text{Mn}_{1.4}\text{O}_4$ (P)	CuCr_2O_4	Tandem
0.966	0.958	0.972	0.970	0.955

3.2. Temperature dependence of the normal spectral emissivities

Fig. 3 shows the normal spectral emissivity as a function of temperature for all samples. The substrate shows the general behavior predicted for metallic materials by the electromagnetic theory, decreasing with increasing wavelength and with a slight increase with temperature in the long-wavelength region [31,32]. This weak temperature dependence is typical for heavily alloyed metals. Very similar results were observed for the normal spectral emissivity of a brushed Inconel 718 sample, with values of 0.4 at short wavelengths and 0.1 at longer ones [34].

The measurement of the emissivity of the substrate is deemed necessary because the substrate may bear significant influence on the emissivity of the materials through a certain degree of semitransparency, especially for aged or thin coatings [22,24]. Substrate measurements were performed in vacuum, as no signs of oxidation were found in the substrates used for these coatings in previous studies, except for heavily aged Pyromark [9,10]. Therefore, the use of vacuum for the uncoated substrate sample was necessary in order to have comparable data in a surface state as close as possible to the one found at working conditions.

Concerning the coatings, their emissivities are all relatively similar and much higher than that of the substrate. Whereas the emissivity of Pyromark does not show any significant temperature dependence, those of all the other coatings experience an increase with temperature. Temperature-independent spectral behaviors of Pyromark have been reported, although the choice of substrate was also found to induce systematic differences in the normal spectral

emissivity among samples [22]. The temperature dependences of the new coatings are mainly observed at wavelengths below $8\ \mu\text{m}$, which can be due to the thermal evolution of the intrinsic optical properties of their oxide nanoparticles. They have been deemed to be repeatable within the experimental uncertainty, and thus are not a consequence of microstructural evolution or degradation. A possible substrate-induced origin for these observations is discouraged due to the absence of any substantial increase in the emissivity of the substrate at such wavelengths. Out of all the measured coatings, the behavior of the $\text{Cu}_{0.5}\text{Cr}_{1.1}\text{Mn}_{1.4}\text{O}_4$ (P) (Fig. 3d) sample has the largest temperature dependence, showing an increasing emissivity with temperature throughout the entire spectral range. To sum up, the results suggest that differences in composition are not the most relevant source of high-temperature emissivity variations and that similarly deposited coatings have comparable normal spectral emissivity values.

In addition, the results in Fig. 3 indicate, as was shown previously for solar selective coatings [12], that the common practice of obtaining high-temperature emissivity spectra by extrapolations from room-temperature data does not account, in general, for the possible temperature dependence of the properties of the coating. In the case of the present work, it can be clearly seen that only Pyromark shows a relatively constant emissivity with temperature. It is important to note that most evolution in the spectra corresponding to the other coatings takes place at shorter wavelengths, where most thermal radiation is emitted at high temperatures.

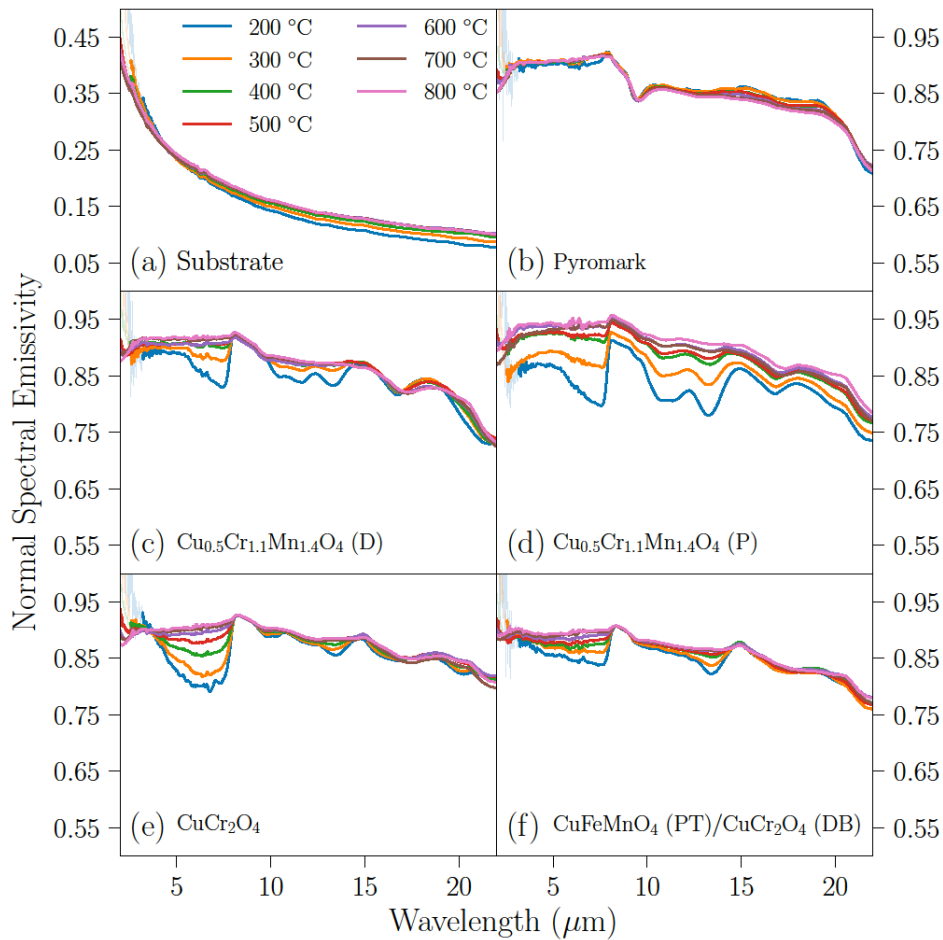


Fig. 3: Normal spectral emissivities of the six samples as a function of temperature between 2 and $22\ \mu\text{m}$. Note the different scales for the emissivity of the substrate and those of the coatings. Noisy data in the short-wavelength region has been shadowed for all samples to improve clarity.

3.3. Directional spectral emissivities

Directional spectral emissivity measurements for all samples are shown in Fig. 4. The highest temperature measured (800 °C) has been chosen to illustrate the main properties of the directional spectra of the materials, as it corresponds to a temperature close to that which is desired to achieve in future applications. In any case, similar directional dependences have been observed at all temperatures.

The directional emissivity of the substrate increases with the emission angle in the way that is expected for a metallic material and reaches its maximum value at around 70° to 80°, depending on wavelength. In the case of the coatings, their angular dependences are remarkably similar. The high values they all feature in the normal direction remain nearly constant up to 50° and then decrease to reach an average value of 0.4 at 80°. In the case of the $\text{Cu}_{0.5}\text{Cr}_{1.1}\text{Mn}_{1.4}\text{O}_4$ (P) coating, its emissivity is slightly higher than that of the other samples in the normal direction but begins a faster decrease at an angle of only 40°. This anomalous angular dependence implies that at 60° the value of its emissivity is almost half of that of the corresponding value for its dense counterpart ($\text{Cu}_{0.5}\text{Cr}_{1.1}\text{Mn}_{1.4}\text{O}_4$ (D)), although the emissivity at 80° is similar to that of the other coatings. For this coating, the spectral curves also show a crossover in the angular dependence, with an emissivity curve for 80° that is larger than for 70° at wavelengths longer than 5 μm . This result is far from the predictions of the electromagnetic theory for bulk homogeneous materials and ideal surfaces [31,32]. A possible explanation relies on the fact that the dominant absorption mechanism in the porous coating is due to surface roughness [9,10], a mechanism of optical absorption that is well known to lose effectiveness at larger angles. In the case of the other materials, their bulk absorption is stronger due to their higher density and their decrease with angle is therefore less pronounced. However, at 80° the emissivity of the substrate becomes dominant for all coatings due to their increased transparency at high angles, which accounts for the similarities among all emissivity spectra of the coatings to that of the substrate.

Furthermore, some common spectral features are observed for all coatings in varying degrees, such as the 8-10 μm shoulder and the 3, 15 and 20 μm peaks for high angles. Their presence for all materials suggests an origin common to all of them which is not to be found on their intrinsic optical properties. Indeed, similar absorption bands can be found in the infrared spectrum of silica glass [35], which is present in all coatings as a binder phase. The band at $\sim 9 \mu\text{m}$ has been observed before for some Pyromark samples depending on the substrate used [22]. Differences among samples in that study were traced back to the use of different substrates, but this correlation suggests that differences in the small secondary phases might be even more important. It is not uncommon for complex materials to reveal specific spectral signatures and peaks only when emitting at oblique angles, due to the different optical properties and directional dependence of their constituents [13]. These non-ideal behaviors highlight the importance of microstructure in determining the thermal radiative properties of porous materials and hint at the possibility of tuning them to improve their performance in heat transfer applications [36].

In order to better visualize the behaviors discussed above, directional spectral values at two discrete wavelengths for both $\text{Cu}_{0.5}\text{Cr}_{1.1}\text{Mn}_{1.4}\text{O}_4$ samples (dense and porous) have been plotted in Fig. 5. These two samples have been selected to check the influence of the microstructure in the directional emissivity of samples with the same composition. It can be seen that both

materials show similar angular dependences at both wavelengths, but that non-ideal tendencies are more significant for the porous sample. This is best observed at $8\ \mu\text{m}$ above 60° , where the emissivity of the porous sample decreases faster than the predictions of the electromagnetic theory for dielectric materials up to 70° and then increases again at 80° . On the contrary, the emissivity of the dense sample remains relatively constant up to 60° and then decreases rapidly to zero only above 70° , in agreement with the theoretical predictions. The differences at $3\ \mu\text{m}$ are much less pronounced due to the fact that this wavelength corresponds to one of the infrared active modes of the silica glass binder, and therefore experiences higher emissivities throughout the angular range.

Some attempts at describing the directional emissivity of materials with complex geometry, such as packed beds of spheres or agglomerated nanoparticles, have been made using the radiative transfer equation (RTE) and Mie's theory [37]. However, agreement of the predicted behavior to the experimental data has been relatively poor, especially at high angles of incidence [38]. A qualitative picture of the sharp decrease of emissivity with the emission angle can be formed by considering shadowing effects, where normally incident light is trapped by multiple reflections inside the geometric features of these systems, but the emission at oblique angles of incidence interacts with an effectively smoother surface, since most of the texture is not accessible from those angles. Shadowing effects are known to be key for the thermal radiative properties of other complex systems, such as V-grooves or foams [39,40]. This point serves to demonstrate that directional selectivity can be inherently induced by the same mechanisms responsible for enhanced light trapping and increased efficiency in the normal direction. Nevertheless, the absence of theoretical tools for calculations of the radiative properties of these type of materials ensures that experimental measurements will continue to be essential for their development in applications.

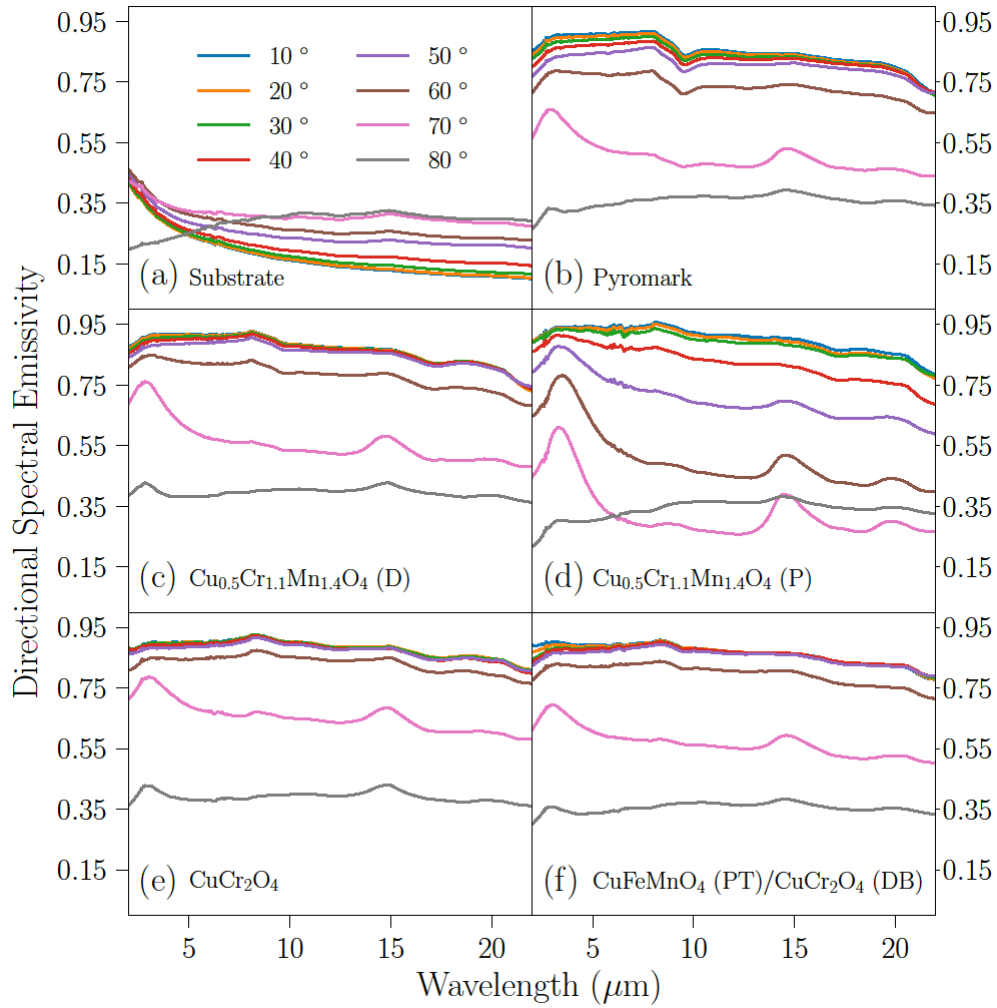


Fig. 4: Directional spectral emissivities at 800 °C for all six samples between 2 and 22 μm .

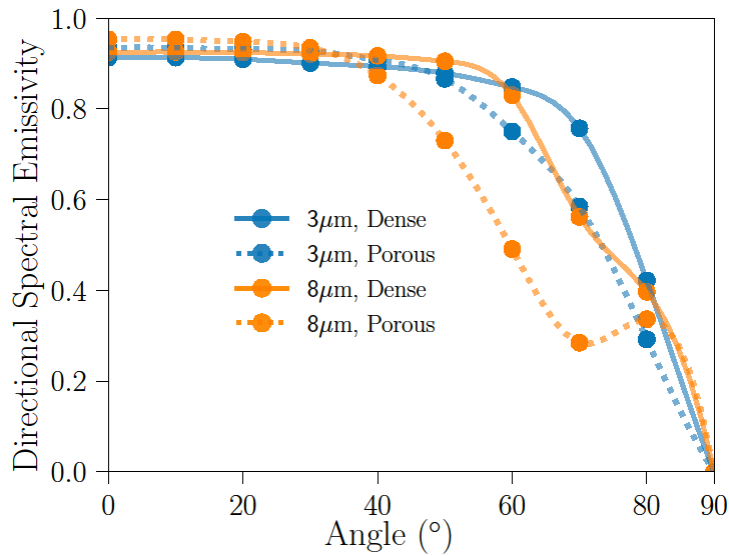


Fig. 5: Comparison of the directional spectral emissivities (800 °C) of the two $\text{Cu}_{0.5}\text{Cr}_{1.1}\text{Mn}_{1.4}\text{O}_4$ coatings (dense and porous) at two wavelengths. The values at 0° and 90° have been set to the values predicted by the electromagnetic theory [31,32].

3.4. Total hemispherical emissivities

The total hemispherical emissivity is the key parameter for solar-to-thermal efficiency estimations, because it controls the total amount of heat lost by thermal radiation at high temperatures [22]. It can be calculated by numerical integration in both wavelength and solid angle of the temperature-dependent spectral directional data shown in previous sections, according to the procedure described in Section 2.3. Results of the integration for the substrate and the coatings are shown in Figs. 6 and 7, respectively.

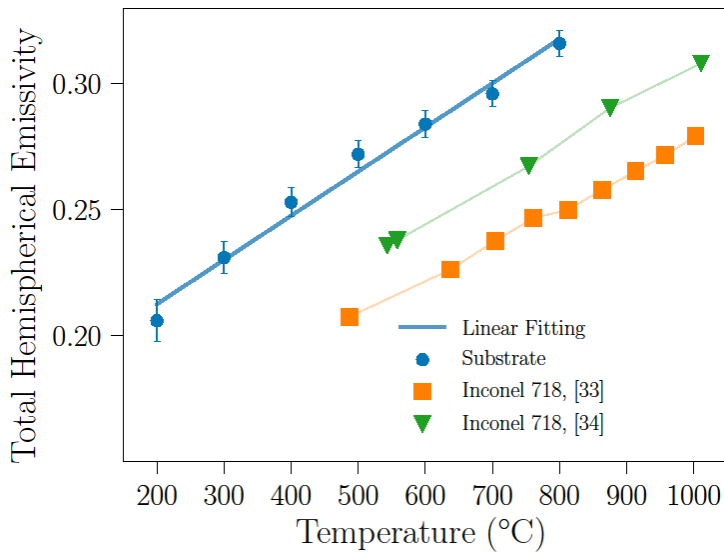


Fig. 6: Total hemispherical emissivity of the substrate fitted to a linear functional form, together with the prediction from free-electron theory [41] with electrical resistivity data for Inconel 625 taken from [42]. Literature data on Inconel 718 [43,44] are shown for comparison. Error bars correspond to standard uncertainty values.

As can be seen in Fig. 6, the total hemispherical emissivity of the Inconel 625 substrate increases linearly, as is typical for metallic materials. These results have been compared to those predicted by the free-electron theory [41], calculated using experimental resistivity for Inconel 625 taken from [42]. Literature data on a similar alloy (Inconel 718) [43,44] are also shown in the same figure for comparison. All measurements have been performed in vacuum, although the surface conditions may differ significantly among samples. An agreement between the slopes of the three datasets is found, despite the differences in composition. The observed offset with the literature data, while significant, is comparable to that among the data for Inconel 718 themselves. Surface contamination, roughness, differences in heat treatment, and the presence of different amounts of secondary phases might explain these discrepancies between literature data. It should be noted that both Inconel alloys are age-hardenable, which means that their microstructure is susceptible to precipitation of secondary phases at high temperature.

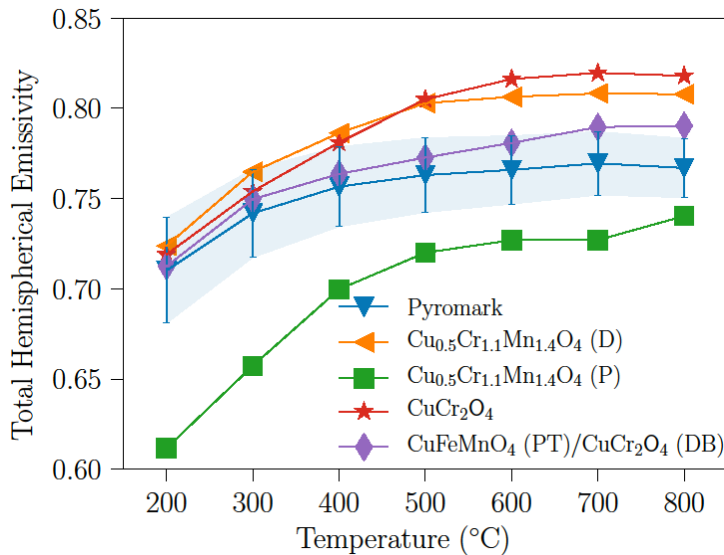


Fig. 7: Total hemispherical emissivities of the five coatings as a function of temperature. Error bars correspond to standard uncertainty values. They have been applied only to Pyromark to improve the clarity of the diagram, due to the small differences in uncertainties among samples.

In the case of the coatings, it is observed (Fig. 7) that in all cases their total hemispherical emissivities increase up to around 500 °C and then mostly stabilize. As expected from the directional data, the Cu_{0.5}Cr_{1.1}Mn_{1.4}O₄ (P) sample is again an exception to the general rule, with a total hemispherical emissivity that is significantly lower than any of the other samples at all temperatures. As discussed above, the strong angular dependence of this sample is the key to its overall reduced heat losses and degree of directional selectivity. It boasts the highest solar absorptance and the highest normal emissivity at high temperature of the entire set of samples, but its emission at off-normal angles is significantly inhibited by a fast decrease of the directional emissivity. This translates into a structure with a reduced total hemispherical emissivity, which may be a strategy worth pursuing in the design of new materials.

The optical properties of the Cu_{0.5}Cr_{1.1}Mn_{1.4}O₄ (P) sample can be regarded as typical of a directionally selective surface, a topic of great interest due to the potential of tuning the emissivity of materials to emit preferentially in a given direction [45]. Surfaces with this property can offer an increase in efficiency by limiting the amount of heat lost by radiation at non-normal directions. Crucially, this improved efficiency does not degrade at high temperatures, compared to the more common spectrally selective surfaces [46]. Many strategies for making directionally selective materials have been studied, such as photonic crystals [47-49], V-grooves [40,50], optical cavities [51,52] and metamaterials [53-55]. Contrary to those approaches, the directional selectivity obtained in this study is achieved directly as part of the spray deposition method, with the associated reduction in costs.

The behavior of the other coatings is much similar among themselves, especially at low temperatures. Nevertheless, some tendencies can be observed. The Cu_{0.5}Cr_{1.1}Mn_{1.4}O₄ (D) and CuCr₂O₄ coatings, which are the most similar samples regarding microstructure, also feature close total hemispherical emissivity values for the entire temperature range, bearing the highest overall values at high temperatures. Meanwhile, the tandem coating features emissivities much closer to those of Pyromark, which correspond to the intermediate values between the Cu_{0.5}Cr_{1.1}Mn_{1.4}O₄ (P) and the CuCr₂O₄, albeit closer to the latter. This is expected, since most of

the tandem structure consists of a denser microstructure, with only the top 5 μm corresponding to a porous layer [9,10].

As the last part of this section, the Pyromark sample has been used as a benchmark for verification of the obtained results and discussion of the variability of literature data. A substantial amount of data on the radiative properties of this paint is available in both the scientific and technical literature, although with a well-known dispersion of values, few reported uncertainties, and mostly in the normal direction [7,20-24]. It is important to note that the total hemispherical emissivity is the only parameter that accounts for all contributions to the radiative heat losses. Temperature-dependent total normal and total hemispherical experimental data have been separately reported in the literature [21-23], but no references containing both total normal and total hemispherical measurements for the same samples have been found. A comparison of the data contained in this work to available literature data from [21-23] is given in Figs. 8 (for the total normal emissivity) and 9 (for the total hemispherical).

A qualitative agreement can be observed for both quantities, although the aforementioned dispersion of values is evident. Most total normal emissivity datasets shown in Fig. 8 feature a positive temperature dependence similar to the data contained in this work, although a negative one has also been found (set 2 from Ref. [23]). In the case of the total hemispherical emissivity (Fig. 9), data from Ref. [23] agree somewhat with the present results, while those of Ref. [22] show a qualitatively similar but much higher total hemispherical emissivity. The discrepancies between datasets, the effects of extrinsic factors (such as morphology and heat treatment) and the difficulty of finding reliable emissivity data for Pyromark have been previously discussed [23]. It should be noted that not all measurements have been performed using the same methods. The data by Höser et al. [21] have been obtained using an infrared camera in the 8-14 μm range, while data in Ref. [23] have been theoretically extrapolated from normal data obtained indirectly using reflectivity measurements. The latter is also the most discrepant dataset, which may be partly explained by the observed variability of samples deposited on different substrates. Overall, this brief comparison highlights the significance of direct emissivity measurements at working temperatures and the need for accurate characterization of materials.

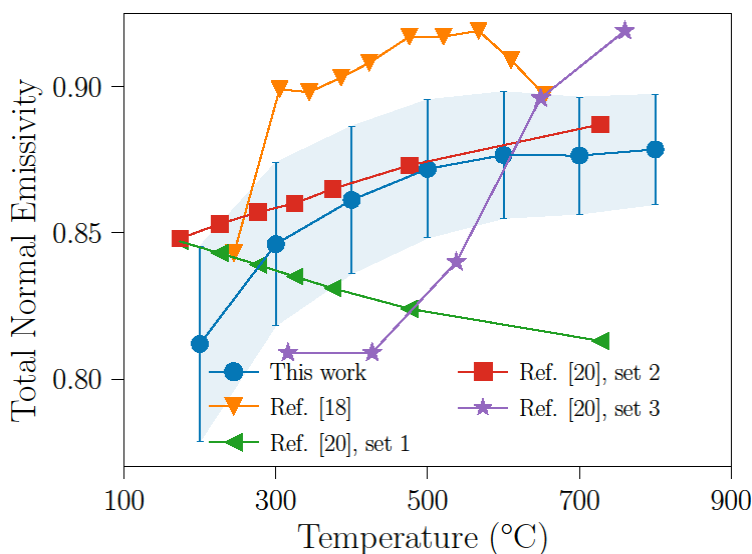


Fig. 8: Total normal emissivity of Pyromark reported in this work compared to data from the literature [18,20]. Error bars correspond to standard uncertainty values.

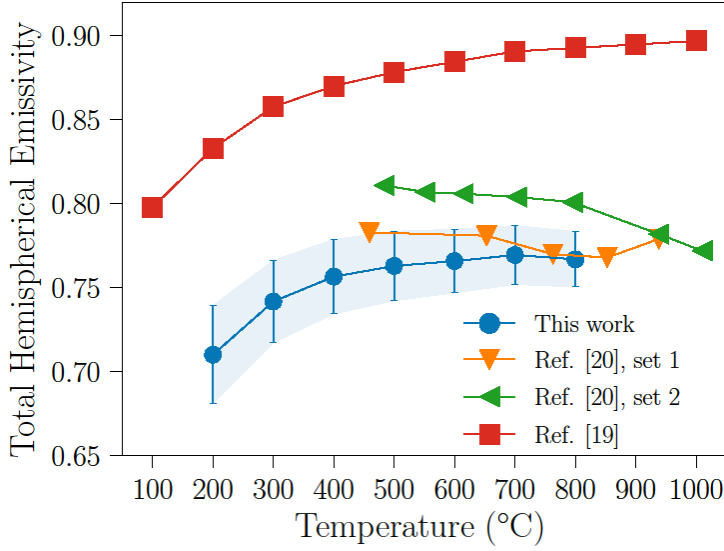


Fig. 9: Total hemispherical emissivity of Pyromark reported in this work compared to that calculated from total normal measurements [19] and compiled data [20]. Error bars correspond to standard uncertainty values.

3.5. Efficiency of the coatings

EVERYTHING DOWN FROM HERE NEEDS TO BE MODIFIED EXTENSIVELY

Accurate temperature-dependent emissivity data allow for estimations of the real efficiency of the materials in CSP applications. Assuming that all heat transfer occurs by radiation, the efficiency of the solar receiver can be formulated through a net energy balance calculation, in which both absorption of solar radiation and its effective retention (by limiting the re-emission of the collector) need to be taken into account. The critical material parameters in this respect are the solar-weighted normal absorptance (α_s) and the total hemispherical emissivity (ε_H) of the coatings, whereas the concentration factor and the temperature of the collector represent the main characteristics of the CSP application. The solar-to-thermal efficiencies can be calculated using the following Eq. (1) [56]:

$$\eta(T) = \alpha_s - \frac{\varepsilon_H(T)\sigma T^4}{CI} \quad (1)$$

where C is the concentration factor (number of suns), I is the solar irradiance (taken as 1000 W/m^2), σ is the Stefan–Boltzmann constant and T is the absolute surface temperature in K. In this indicator, the parameters are already spectrally integrated and the directionality of the thermal emission has been taken into account.

A temperature of $800 \text{ }^\circ\text{C}$ and concentration factors around 1000 suns have been selected in order to comply with the expected aims of future solar tower plants [8].

On a final note, it should be borne in mind that neither a possible temperature dependence of the absorptivity or the effects of aging in the emissivity at high temperatures have been discussed. Further studies in this direction are therefore desirable.

4. Conclusions

Infrared emissivity measurements have been performed in a set of alternative coatings developed with the aim of increasing the working temperature and lifetime of CSP systems. The

metallic substrate and Pyromark paint deposited in the same conditions have also been evaluated as control samples. The main conclusions are:

- The emissivities of most coatings are very similar and comparable to Pyromark, which makes them valid alternatives to the latter at temperatures at which it rapidly degrades.
- Stronger temperature dependences have been observed for the emissivities of the alternative coatings compared to Pyromark, which reflects the importance of high-temperature measurements.
- The most deviant sample is the porous $\text{Cu}_{0.5}\text{Cr}_{1.1}\text{Mn}_{1.4}\text{O}_4$ coating, due to differences in morphology and surface structure. This type of techniques can be employed to tune thermal radiative properties of materials.
- Overall, structural parameters bear more significant influence than composition in determining the emissivity of these black coatings. This is also true for Pyromark, as revealed by the considerable dispersion of literature data.

Acknowledgments

The support of this research by Department of Energy through DOE SunShot Project ([DE-EE0005802](#)) is acknowledged. I. González de Arrieta would like to acknowledge the Basque Government for its support through a PhD fellowship.

References

- [1] U. Pelay, L. Luo, Y. Fan, D. Stitou, M. Rood, Thermal energy storage systems for concentrated solar power plants, *Renew. Sustain. Energy Rev.* 79 (2017) 82-100. doi:10.1016/j.rser.2017.03.139.
- [2] S. Chu, A. Majumdar, Opportunities and challenges for a sustainable energy future, *Nature* 488 (2012) 294–303. doi:10.1038/nature11475.
- [3] A. Dan, H.C. Barshilia, K. Chattopadhyay, B. Basu, Solar energy absorption mediated by surface plasma polaritons in spectrally selective dielectric-metal-dielectric coatings: A critical review, *Renew. Sustain. Energy Rev.* 79 (2017) 1050-1077. doi:10.1016/j.rser.2017.05.062.
- [4] J. Moon, D. Lu, B. VanSaders, T.K. Kim, S.D. Kong, S. Jin, R. Chen, Z. Liu, High performance multi-scaled nanostructured spectrally selective coating for concentrating solar power, *Nano Energy.* 8 (2014) 238-246. doi:10.1016/j.nanoen.2014.06.016.
- [5] E. Sani, E. Landi, D. Sciti, V. Medri, Optical properties of ZrB₂ porous architectures, *Sol. Energy Mater. Sol. Cells.* 144 (2016) 608-615. doi:10.1016/j.solmat.2015.09.068.
- [6] G. Pellegrini, Experimental methods for the preparation of selectively absorbing textured surfaces for photothermal solar conversion, *Sol. Energy Mater.* 3 (3) (1980) 391-404. doi:10.1016/0165-1633(80)90028-3.
- [7] A. Boubault, C.K. Ho, A. Hall, T.N. Lambert, A. Ambrosini, Durability of solar absorber coatings and their cost-effectiveness, *Sol. Energy Mater. Sol. Cells.* 166 (2017) 176-184. doi:10.1016/j.solmat.2017.03.010.

- [8] M. Mehos, C. Turchi, J. Vidal, M. Wagner, Z. Ma, C. Ho, W. Kolb, C. Andraka, A. Kruiženga, Concentrating Solar Power Gen3 Demonstration Roadmap, NREL (National Renewable Energy Laboratory (NREL), Golden, CO (United States)) (2017)
- [9] T.K. Kim, B. VanSaders, E. Caldwell, S. Shin, Z. Liu, S. Jin, R. Chen, Copper-alloyed spinel black oxides and tandem-structured solar absorbing layers for high-temperature concentrating solar power systems, *Sol. Energy*. 132 (2016) 257-266. doi:10.1016/j.solener.2016.03.007.
- [10] E.B. Rubin, Y. Chen, R. Chen, Optical properties and thermal stability of Cu spinel oxide nanoparticle solar absorber coatings, *Sol. Energy Mater. Sol. Cells*. 195 (2019) 81-88. doi:10.1016/j.solmat.2019.02.032.
- [11] I. Setién-Fernández, T. Echániz, L. González-Fernández, R.B. Pérez-Sáez, E. Céspedes, J.A. Sánchez-García, L. Álvarez-Fraga, R. Escobar Galindo, J.M. Albella, C. Prieto, M.J. Tello, First spectral emissivity study of a solar selective coating in the 150-600°C temperature range, *Sol. Energy Mater. Sol. Cells*. 117 (2013) 390-395. doi:10.1016/j.solmat.2013.07.002.
- [12] T. Echániz, I. Setién-Fernández, R.B. Pérez-Sáez, C. Prieto, R.E. Galindo, M.J. Tello, Importance of the spectral emissivity measurements at working temperature to determine the efficiency of a solar selective coating, *Sol. Energy Mater. Sol. Cells*. 140 (2015) 249-252. doi:10.1016/j.solmat.2015.04.009.
- [13] A. Dan, B. Basu, T. Echániz, I. González de Arrieta, G.A. López, H.C. Barshilia, Effects of environmental and operational variability on the spectrally selective properties of W/WAIN/WAION/Al₂O₃-based solar absorber coating, *Sol. Energy Mater. Sol. Cells*. 185 (2018) 342-350. doi:10.1016/j.solmat.2018.04.020.
- [14] E.T. Kwor, S. Mattei, Emissivity measurements for Nextel Velvet Coating 811-21 between -36 °C and 82 °C, *High Temp. - High Press*. 33(5) (2001) 551-556. doi:10.1068/htwu385.
- [15] R. Brandt, C. Bird, G. Neuer, Emissivity reference paints for high temperature applications, *Meas. J. Int. Meas. Confed*. 41 (7) (2008) 731-736. doi:10.1016/j.measurement.2007.10.007.
- [16] D. Cárdenas-García, C. Monte, Bilateral Intercomparison of Spectral Directional Emissivity Measurement Between CENAM and PTB, *Int. J. Thermophys*. 35 (6-7) (2014) 1299–1309. doi:10.1007/s10765-014-1686-1.
- [17] A. Adibekyan, E. Kononogova, C. Monte, J. Hollandt, High-Accuracy Emissivity Data on the Coatings Nextel 811-21, Herberts 1534, Aeroglaze Z306 and Acktar Fractal Black, *Int. J. Thermophys*. 38 (2017) 89. doi:10.1007/s10765-017-2212-z.
- [18] P. Honnerová, J. Martan, M. Kucera, M. Honner, J. Hameury, New experimental device for high-temperature normal spectral emissivity measurements of coatings, *Meas. Sci. Technol*. 25 (9) (2014) 095501. doi:10.1088/0957-0233/25/9/095501.
- [19] P. Honnerová, J. Martan, M. Honner, Uncertainty determination in high-temperature spectral emissivity measurement method of coatings, *Appl. Therm. Eng*. 124 (2017) 261-270. doi:10.1016/j.applthermaleng.2017.06.022.

- [20] J. Fang, N. Tu, J. Wei, X. Du, Effects of surface optical and radiative properties on the thermal performance of a solar cavity receiver, *Sol. Energy*. 171 (2018) 157-170. doi:10.1016/j.solener.2018.06.075.
- [21] D. Höser, R. Wallimann, P.R. von Rohr, Uncertainty Analysis for Emissivity Measurement at Elevated Temperatures with an Infrared Camera, *Int. J. Thermophys.* 37 (2016) 14. doi:10.1007/s10765-015-2022-0.
- [22] C.K. Ho, A.R. Mahoney, A. Ambrosini, M. Bencomo, A. Hall, T.N. Lambert, Characterization of Pyromark 2500 Paint for High-Temperature Solar Receivers, *J. Sol. Energy Eng.* 136 (1) (2013) 014502. doi:10.1115/1.4024031.
- [23] J.M. Suo-Anttila, J.T. Nakos, W. Gill, Shroud boundary condition characterization experiments at the Radiant Heat Facility., Albuquerque, NM, and Livermore, CA, 2004. doi:10.2172/919650.
- [24] J. Coventry, P. Burge, Optical properties of Pyromark 2500 coatings of variable thicknesses on a range of materials for concentrating solar thermal applications, *AIP Conf. Proc.* 1850 (2017) 030012. doi:10.1063/1.4984355.
- [25] J. Moon, T. Kyoung Kim, B. VanSaders, C. Choi, Z. Liu, S. Jin, R. Chen, Black oxide nanoparticles as durable solar absorbing material for high-temperature concentrating solar power system, *Sol. Energy Mater. Sol. Cells.* 134 (2015) 417-424. doi:10.1016/j.solmat.2014.12.004.
- [26] L. Del Campo, R.B. Pérez-Sáez, X. Esquisabel, I. Fernández, M.J. Tello, New experimental device for infrared spectral directional emissivity measurements in a controlled environment, *Rev. Sci. Instrum.* 77 (2006) 113111. doi:10.1063/1.2393157.
- [27] R.B. Pérez-Sáez, L. Del Campo, M.J. Tello, Analysis of the accuracy of methods for the direct measurement of emissivity, *Int. J. Thermophys.* 29 (3) (2008) 1141–1155. doi:10.1007/s10765-008-0402-4.
- [28] L. González-Fernández, R.B. Pérez-Sáez, L. del Campo, M.J. Tello, Analysis of calibration methods for direct emissivity measurements, *Appl. Opt.* 49 (14) (2010) 2728-2735. doi:10.1364/AO.49.002728.
- [29] L. Del Campo, R.B. Pérez-Sáez, L. González-Fernández, M.J. Tello, Combined standard uncertainty in direct emissivity measurements, *J. Appl. Phys.* 107 (2010) 113510. doi:10.1063/1.3431541.
- [30] T. Echániz, R.B. Pérez-Sáez, M.J. Tello, IR radiometer sensitivity and accuracy improvement by eliminating spurious radiation for emissivity measurements on highly specular samples in the 2–25 μm spectral range, *Meas. J. Int. Meas. Confed.* 110 (2017) 22-26. doi:10.1016/j.measurement.2017.06.010.
- [31] R. Siegel, J.R. Howell, *Thermal radiation heat transfer - Third Edition*, 1992.
- [32] M.F. Modest, *Radiative Heat Transfer: Second Edition*, 2003. doi:10.1016/B978-0-12-503163-9.X5000-0.
- [33] C. Monte, J. Hollandt, The determination of the uncertainties of spectral emissivity measurements in air at the PTB, *Metrologia*. 47 (2) (2010) S172. doi:10.1088/0026-1394/47/2/S14.

- [34] L. del Campo, R.B. Pérez-Sáez, L. González-Fernández, X. Esquisabel, I. Fernández, P. González-Martín, M.J. Tello, Emissivity measurements on aeronautical alloys, *J. Alloy. Compd.* 489 (2) (2010) 482-487. doi:10.1016/j.jallcom.2009.09.091.
- [35] R. Kitamura, L. Pilon, M. Jonasz, Optical constants of silica glass from extreme ultraviolet to far infrared at near room temperature, *Appl. Opt.* 46 (2007) 8118-8133. doi:10.1364/AO.46.008118
- [36] B. Rousseau, S. Guevelou, A. Mekeze-Monthe, J. Vicente, L. Del Campo, D. De Sousa Meneses, P. Echegut, C. Caliot, G. Flamant, Tuning the spectral emittance of a-SiC open-cell foams up to 1300 K with their macro porosity, *AIP Adv.* 6 (2016) 065226. doi:10.1063/1.4955142.
- [37] J.F. Sacadura, Thermal radiative properties of complex media: Theoretical prediction versus experimental identification, *Heat Transf. Eng.* 32 (9) (2011) 754-770. doi:10.1080/01457632.2011.525140.
- [38] R. Lopes, L. s M. Moura, D. Baillis, J.-F. Sacadura, Directional Spectral Emittance of a Packed Bed: Correlation Between Theoretical Prediction and Experimental Data, *J. Heat Transfer.* 123 (2) (2001) 240-248. doi:10.1115/1.1338134.
- [39] Y. Li, X.L. Xia, C. Sun, Q. Ai, B. Liu, H.P. Tan, Tomography-based analysis of apparent directional spectral emissivity of high-porosity nickel foams, *Int. J. Heat Mass Transf.* 118 (2018) 402-415. doi:10.1016/j.ijheatmasstransfer.2017.11.005.
- [40] R.B. Mulford, N.S. Collins, M.S. Farnsworth, M.R. Jones, B.D. Iverson, Total hemispherical apparent radiative properties of the infinite V-groove with specular reflection, *Int. J. Heat Mass Transf.* 124 (2018) 168-176. doi:10.1016/j.ijheatmasstransfer.2018.03.041.
- [41] A.J. Sievers, Thermal radiation from metal surfaces, *J. Opt. Soc. Am.* 68 (11) (1978) 1505-1516. doi:10.1364/JOSA.68.001505.
- [42] K. D. Maglić, N. Lj. Perović, A. M. Stanimirović, Calorimetric and transport properties of Zircalloy 2, Zircalloy 4, and Inconel 625, *Int. J. Thermophys.* 15 (4) (1994) 741-755. doi:10.1007/BF01563797
- [43] B.P. Keller, S.E. Nelson, K.L. Walton, T.K. Ghosh, R. V Tompson, S.K. Loyalka, Total hemispherical emissivity of Inconel 718, *Nucl. Eng. Des.* 287 (2015) 11–18. doi:10.1016/j.nucengdes.2015.02.018.
- [44] G.A. Greene, C.C. Finrock, T.F. Irvine, Total hemispherical emissivity of oxidized Inconel 718 in the temperature range 300-1000 °C, *Exp. Therm. Fluid Sci.* 22 (2000) 145–153. doi:10.1016/S0894-1777(00)00021-2.
- [45] V. Badescu, Spectrally and angularly selective photothermal and photovoltaic converters under one-sun illumination, *J. Phys. D: Appl. Phys.* 38 (2005) 2166. doi:10.1088/0022-3727/38/13/014.
- [46] M.J. Blanco, J.G. Martín, D.C. Alarcón-Padilla, Theoretical efficiencies of angular-selective non-concentrating solar thermal systems, *Sol. Energy.* 76 (6) (2004) 683-691. doi:10.1016/j.solener.2004.01.005.
- [47] R.E. Hamam, I. Celanovic, M. Soljagic, Angular photonic band gap, *Phys. Rev. A.* 83 (2011) 035806. doi:10.1103/PhysRevA.83.035806.

- [48] Y. Shen, D. Ye, I. Celanovic, S.G. Johnson, J.D. Joannopoulos, M. Soljacic, Optical broadband angular selectivity, *Science*. 343 (6178) (2014) 1499-1501. doi:10.1126/science.1249799.
- [49] M. Florescu, H. Lee, I. Puscasu, M. Pralle, L. Florescu, D. Z. Ting, J.P. Dowling, Improving solar cell efficiency using photonic band-gap materials, *Sol. Energy Mater. Sol. Cells*. 91 (17) (2007) 1599-1610. doi:10.1016/j.solmat.2007.05.001.
- [50] K.G.T. Hollands, Directional selectivity, emittance, and absorptance properties of vee corrugated specular surfaces, *Sol. Energy*. 7 (3) (1963) 108-116. doi:10.1016/0038-092X(63)90036-7.
- [51] L. Weinstein, D. Kraemer, K. McEnaney, G. Chen, Optical cavity for improved performance of solar receivers in solar-thermal systems, *Sol. Energy*. 108 (2014) 69-79. doi:10.1016/j.solener.2014.06.023.
- [52] L.A. Weinstein, W.C. Hsu, S. Yerci, S. V. Boriskina, G. Chen, Enhanced absorption of thin-film photovoltaic cells using an optical cavity, *J. Opt.* 17 (2015) 055901. doi:10.1088/2040-8978/17/5/055901.
- [53] D. Costantini, A. Lefebvre, A.L. Coutrot, I. Moldovan-Doyen, J.P. Hugonin, S. Boutami, F. Marquier, H. Benisty, J.J. Greffet, Plasmonic metasurface for directional and frequency-selective thermal emission, *Phys. Rev. Appl.* 4 (2015) 014023. doi:10.1103/PhysRevApplied.4.014023.
- [54] E. Sakr, P. Bermel, Thermophotovoltaics with spectral and angular selective doped-oxide thermal emitters, *Opt. Express*. 25 (20) (2017) A880-A895. doi:10.1364/OE.25.00A880.
- [55] H. Wang, V. Prasad Sivan, A. Mitchell, G. Rosengarten, P. Phelan, L. Wang, Highly efficient selective metamaterial absorber for high-temperature solar thermal energy harvesting, *Sol. Energy Mater. Sol. Cells*. 137 (2015) 235-242. doi:10.1016/j.solmat.2015.02.019.
- [56] M.M. Koltun, *Selective Optical Surfaces for Solar Energy Converters*, Allerton Press Inc., New York, 1981, pp. 118-120.